A Letters Journal Exploring the Frontiers of Physics

June 2021

EPL, **134** (2021) 68003 www.epljournal.org
doi: 10.1209/0295-5075/134/68003

Quantification of in-plane flexoelectricity in lipid bilayers

Nidhin Thomas and Ashutosh Agrawal[(a)]

Department of Mechanical Engineering, University of Houston - Houston, TX, 77204, USA

received 1 February 2021; accepted in final form 17 May 2021
published online 17 August 2021

Abstract – Lipid bilayers behave as 2D dielectric materials that undergo polarization and deformation in the presence of an electric field. This effect has been previously modeled by continuum theories which assume a polarization field oriented normal to the membrane surface. However, the molecular architecture of the lipids reveals that the headgroup dipoles are primarily oriented tangential to the membrane surface. Here, we perform atomistic and coarse-grained molecular dynamics simulations to quantify the in-plane polarization undergone by a flat bilayer and a spherical vesicle in the presence of an applied electric field. We use these predictions to compute an effective in-plane flexoelectric coefficient for four different lipid types. Our findings provide the first molecular proof of the in-plane polarization undergone by lipid bilayers and furnish the material parameter required to quantify membrane-electric field interactions.

Introduction. – Lipid membranes are 2D liquid crystal films that define the structural identity of cells and cellular organelles. Similar to 3D liquid crystals, lipids bilayers behave as dielectric materials that undergo polarization and deformation when subjected to electric fields. This electromechanical coupling forms the basis for various phenomena. For example, endogenous electric fields have been shown to play a critical role in wound healing and tissue development [1–3]. Electric-field–induced pore formation in bilayers is widely used to deliver genes and drugs into cells [4–8]. Electroporation is also employed to treat some cancers [9–11]. Electromechanical coupling plays a vital role in regulating the workings of auditory hair cells in mammals [12–14]. Electric-field–induced vesicle deformation has been used to investigate membrane properties and stability [15–18].

Several theories have been proposed over the last two decades to model and comprehend the electromechanical coupling in lipid bilayers, also referred to as flexoelectricity [19–24]. These frameworks have invariably invoked lipid dipoles and the resulting polarization field oriented normal to the membrane surface. However, lipid headgroup structure reveals that lipid dipoles predominantly lie in the tangential plane of the membrane surface. Figure 1 shows the dipole vector in a DPPC lipid. The dipole vector composed of the choline group and the phosphate group is oriented at 71° from the surface normal vector. As a result, the polarization field arising from the reorientation of the dipoles is expected to be primarily in the tangent plane. To incorporate this feature, Steigmann and Agrawal employed the 3D liquid crystal theory to derive a new electromechanical theory with in-plane polarization field [25]. This new model was recently used to predict shape transformations of confined vesicles [26]. While the application of the in-plane flexoelectric model has just begun, a quantification of the in-plane polarization and the required material parameter (in-plane flexoelectric coefficient) for the continuum model is still lacking. Here, in this study, we use atomistic studies and coarse-grained

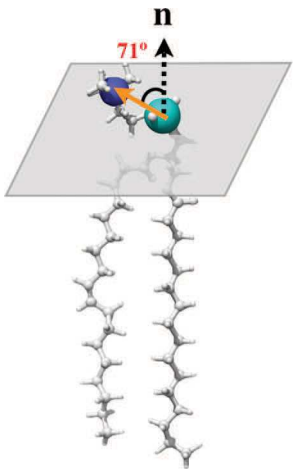

Fig. 1: Lipid headgroup dipole in a POPC lipid (orange vector). Phosphorus and nitrogen atoms are represented by cyan and blue spheres, respectively. The headgroup dipole makes 71° with respect to the bilayer normal, making them essentially parallel to bilayer surface.

[(a)]E-mail: ashutosh@uh.edu (corresponding author)

molecular dynamics to address this issue. Our simulations show that bilayers undergo significant in-plane polarization in the presence of a tangential electric field, yielding the material parameter for four lipid types.

Method. – We adopted two approaches to quantify the in-plane polarization and the in-plane flexoelectric coefficient in lipid bilayers. We simulated all-atom flat bilayers with CHARMM36 and coarse-grained lipid vesicles with CG-MARTINI force field [27,28]. The two systems were subjected to electric fields and the dipole reorientation and effective in-plane polarization were computed. These predictions were then used with the theoretical formulation proposed in [25] to estimate the in-plane flexoelectric coefficient. We used four different lipid types, 1-palmitoyl-2-oleoyl-sn-glycero-3-phosphocholine (POPC), 1,2-dioleoyl-sn-glycero-3-phosphocholine (DOPC), 1,2-dipalmitoyl-sn-glycero-3-phosphocholine (DPPC) and 1-palmitoyl-2-oleoyl-sn-glycero-3-phosphoethanolamine (POPE), to capture the effect of lipid properties on the electromechanical response and the in-plane flexoelectric coefficient.

The all-atom flat bilayers were created using CHARMM-GUI [29,30]. Each leaflet was comprised of 128 lipids and the system was solvated by 50 water molecules per lipid. The bilayers were subjected to electric fields oriented parallel to the bilayer surface and were simulated for at least 300 ns. The coarse-grained flat bilayer and the vesicles were created in CHARMM-GUI Martini Maker. The POPC flat bilayer was composed of 128 lipids and was solvated by 2852 water molecules. The vesicles were made of ∼4500 and ∼3000 lipids in the outer and the inner leaflets. More than 500000 water molecules were used to solvate the vesicles. The flat bilayer was simulated for 5 μs, and the vesicles were simulated for 1 μs. The simulation data from the first 500 ns was discarded from the sampling analysis. The orientation of lipid headgroup dipoles in both the flat bilayers and the lipid vesicles were computed using an in-house code developed in MATLAB. Further details of the systems and the simulation protocols are provided in the Supplementary Material `Supplementarymaterial.pdf` (SM).

Results. –

Predictions from the all-atom simulations. Figure 2 shows the all-atom POPC bilayer and the direction of the applied electric field. Figure 3(a) shows the effect of electric field on the dipole reorientation in the POPC bilayer. In fig. 3(a), the x-axis is the angle (θ) that a dipole vector projected on to the tangent plane makes with the electric field (see fig. 2). Thus, the angle is 0° when the vector is in the direction of the electric field and is 180° when the vector is oriented opposite to the electric field. The y-axis shows the probability density of the lipid dipoles to be oriented in the θ-direction in the entire bilayer.

In the absence of electric field, the dipoles are free to rotate in the tangent plane and hence all the orientations

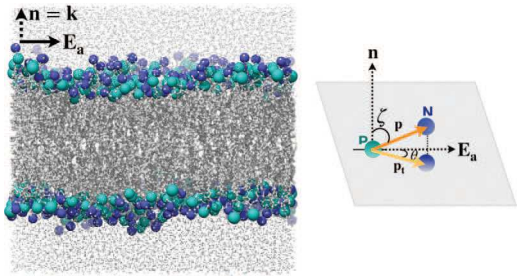

Fig. 2: Simulated atomistic system showing the POPC lipid bilayer subjected to lateral electric field ($\mathbf{E}_a$). Phosphorus and nitrogen atoms of lipid headgroups are represented by cyan and blue colored spheres, respectively. Lipid acyl chains are shown in gray color and water molecules are represented by light gray beads on both sides of the bilayer. ζ is the angle the dipole makes with the bilayer normal and θ is the angle the projected dipole makes with the applied electric field.

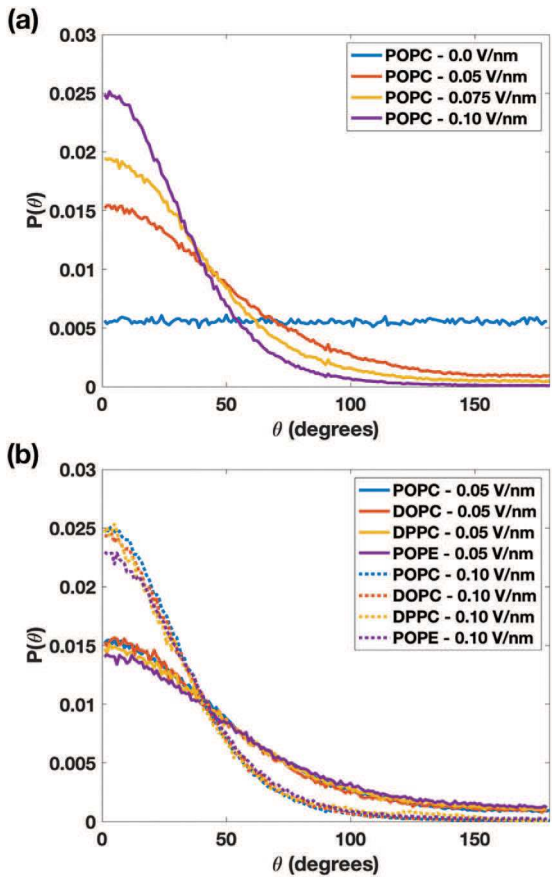

Fig. 3: Electric-field–induced dipole reorientation in flat bilayers (a) Lateral angle probability distribution function ($P(\theta)$) for POPC lipids when subjected to different lateral electric fields. When no electric field is applied, distribution is uniform. When lateral electric field is applied, lipid headgroup dipole vectors begin to orient along the direction of the applied electric field. The reorientation is proportional to the magnitude of the applied electric field. (b) $P(\theta)$ for POPC, DOPC, DPPC and POPE lipids at 0.05 V/nm and 0.10 V/nm electric field values. All four lipids show similar reorientation of the headgroup dipoles.

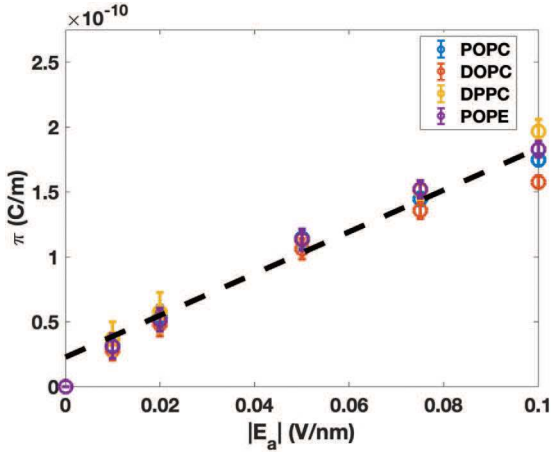

Fig. 4: Magnitude of the in-plane polarization density ($\pi = |\boldsymbol{\pi}|$) as a function of the applied electric field predicted from flat bilayer simulations. Higher electric field leads to higher dipole reorientation and hence, higher π values. A linear fit to the data (black dashed curve) yields an estimate of the in-plane flexoelectric coefficient. Collectively, the four lipids yield an average value of $D \approx 5.77 \times 10^{17}\,\mathrm{Nm/C^2}$. The error bars represent the standard deviation in the polarization densities.

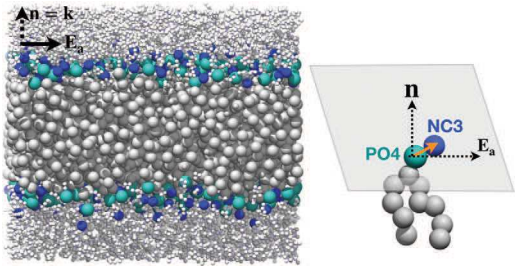

Fig. 5: Coarse-grained POPC bilayer simulated in MARTINI. PO4 and NC3 beads are shown in cyan and blue, respectively. The lipid headgroup dipole (orange vector), as shown in the inset, is drawn from the PO4 bead to the NC3 bead.

have equal probability (blue curve). However, when subjected to increasing electric fields, lipid dipoles begin to preferentially orient along the direction of the electric field. This increases the probability of finding a dipole vector at smaller angles with respect to the electric field direction, resulting in a rise in the $P(\theta)$ curves at smaller angles and a decline at higher angles. Once the electric field reaches 0.1 V/nm, the majority of the dipoles are aligned with the electric field.

To quantify the effect of lateral electric field on different lipid types, we simulate three additional flat bilayers made of DOPC, DPPC and POPE lipids. While POPC has one unsaturated acyl chain, DOPC and DPPC have two and zero unsaturated acyl chains, respectively. POPE lipids, on the other hand, have a different headgroup compared to the PC lipids. The POPE headgroup dipoles make an angle of 77° with respect to the bilayer normal (compared to 71° for POPC lipids). Figure 3(b) shows the probability function for the three lipids at 0.05 V/nm

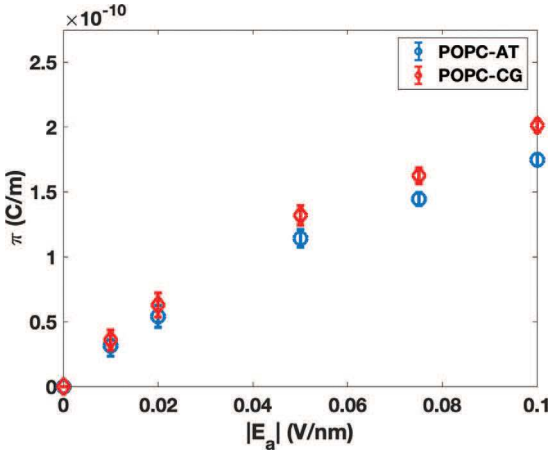

Fig. 6: Comparison of the in-plane polarization densities obtained from the coarse-grained and the all-atom models of the POPC bilayer. The two approaches yield similar values, and the small deviations may be attributed to the differences in the force field parameters.

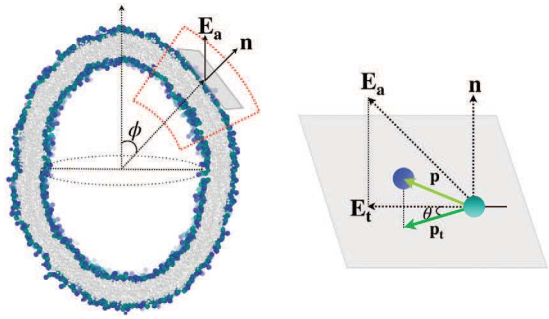

Fig. 7: Coarse-grained POPC vesicle in the presence of an applied electric field (0.025 V/nm). The initial spherical vesicle turns into a prolate ellipsoid in the presence of the electric field. The electric-field–induced reorientation of the dipole vector is captured via the angle θ between the projected dipole vector $\mathbf{p_t}$ and the projected electric field vector $\mathbf{E_t}$ onto the tangent plane of the vesicle surface.

and 0.10 V/nm electric fields. Despite their structural differences, the dipole vectors of all three lipids show similar orientation changes as POPC for the applied electric fields.

We next used the dipole orientations to compute the in-plane polarization density (per unit area) and the in-plane flexoelectric coefficient for the four lipid systems. To compute the local in-plane polarization density in a leaflet, we divide the projected dipole vector by the area of the lipid headgroup. We average this over the two leaflets of the bilayer and sum up the two contributions to compute the resulting in-plane polarization density for the bilayer. Thus, the in-plane polarization density $\boldsymbol{\pi}$ is given by

$$\boldsymbol{\pi} = \left\langle \sum_{i=1}^{2} \mathbf{P}\mathbf{p_i}/A \right\rangle, \tag{1}$$

where $i = \{1, 2\}$ accounts for the two leaflets, $\mathbf{P} = \mathbf{I} - \mathbf{n_i} \otimes \mathbf{n_i} = \mathbf{I} - \mathbf{k} \otimes \mathbf{k}$ is the projection tensor, $\mathbf{p_i}$ is

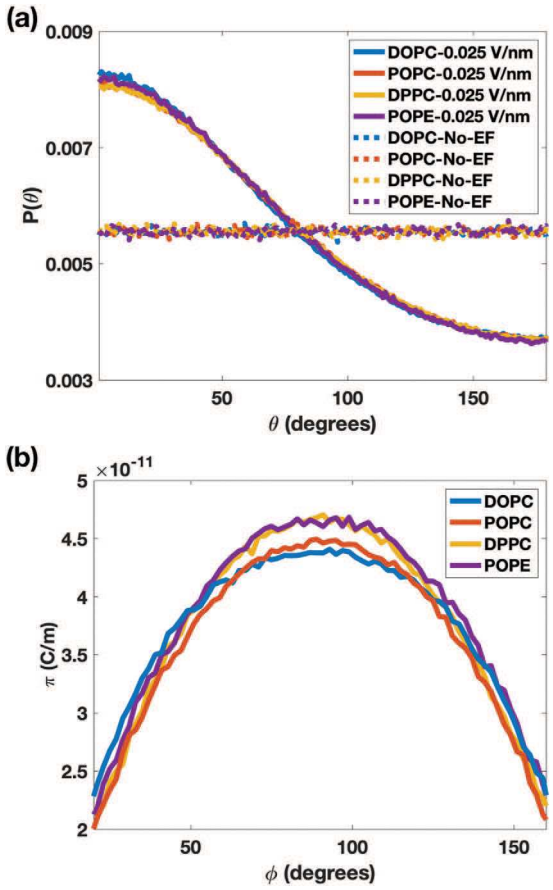

Fig. 8: Predictions from the vesicle simulations. (a) $P(\theta)$ plots for POPC, DOPC, DPPC and POPE lipids in the absence and presence of 0.025 V/nm electric field. In the absence of electric field, $P(\theta)$ plots are flat as dipoles undergo free rotation. In the presence of electric field, dipoles undergo reorientation and $P(\theta)$ increases for smaller angles and decreases for larger angles. The plots show similar trends for all the four lipid types. (b) The magnitude of in-plane polarization density as we move along a meridian from the north pole to the south pole of the deformed vesicle ($20^\circ \leq \phi \leq 160^\circ$). The magnitude increases as we move away from the poles towards the equator, in proportion to the magnitude of the projected electric field onto the tangent plane and the dipole reorientation.

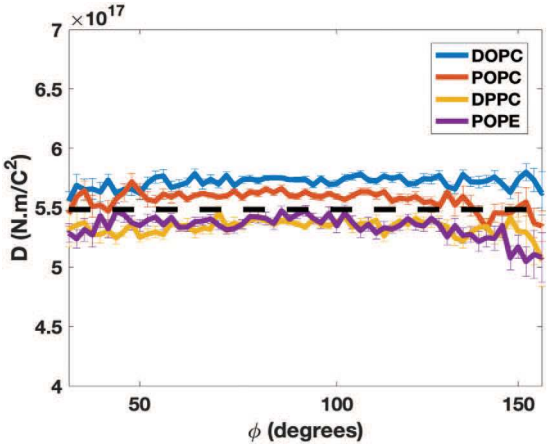

Fig. 9: The predicted in-plane flexoelectric coefficient obtained from the vesicle simulations. These simulations yield an average value of $5.5 \times 10^{17}\,\mathrm{Nm/C^2}$ for the four lipid types (black dashed curve). The error bar represents the standard deviation in the polarization densities.

lipid dipole vector in a leaflet, A is the area per lipid, and $\langle\,\rangle$ represents the averaging performed over the bilayer. Figure 4 shows the magnitude of $\boldsymbol{\pi}$ for the four lipid systems. The polarization density increases with an increase in the magnitude of the applied electric field as more lipids get oriented in the direction of the applied electric field. The four lipid simulations yield similar estimates. The slight drift in the estimated values at 0.1 V/nm could be occurring because of larger fluctuations in the bilayer generated by electric-field–induced compressive in-plane stresses.

Next, we use the estimated in-plane polarization density to compute the in-plane flexoelectric coefficient for the new electromechanical theory with an in-plane polarization field. For such a system, as shown in [25], the membrane energy is given by

$$U = kH^2 + \bar{k}K + \frac{1}{2}D\,|\boldsymbol{\pi}|^2\,, \tag{2}$$

where the first two terms are the classic Helfrich-Canham energy that models the mechanical response of bilayers [31–34] and the third term is the flexoelectric term that depends on the in-plane flexoelectric coefficient D and the in-plane polarization density $\boldsymbol{\pi}$. As shown in [25], equilibrium conditions yield the equation

$$D\boldsymbol{\pi} = \mathbf{P}\,\mathbf{E}_a. \tag{3}$$

We rearrange the above equation to obtain the relation

$$D = \sqrt{\frac{\mathbf{E}_a \cdot \mathbf{P}\,\mathbf{E}_a}{\boldsymbol{\pi}\cdot\boldsymbol{\pi}}}, \tag{4}$$

where we have used the identity $\mathbf{P}^T\mathbf{P} = \mathbf{P}$. For the flat bilayer systems, $\mathbf{P}\mathbf{E}_a = \mathbf{E}_a$. Therefore, the expression for the in-plane flexoelectric coefficient reduces to

$$D = \frac{|\mathbf{E}_a|}{|\boldsymbol{\pi}|}. \tag{5}$$

Thus, the in-plane flexoelectric coefficient is the reciprocal of the slope of the $\pi(|\mathbf{E}_a|)$ curves. The linear fit (black dashed curve) in fig. 4 yields an estimate of $D \approx 5.77 \times 10^{17}\,\mathrm{Nm/C^2}$ for the four simulated lipid types.

Finally, to ensure that the applied electric fields did not compromise the integrity of the bilayers, we calculated the deuterium order parameter of the lipid acyl chains for the POPC, DOPC, DPPC and POPE bilayers. The order parameter shows a monotonic increase with an increase in the applied electric field (fig. S1 in the SM). This implies that the bilayer thickness increases with an increase in the

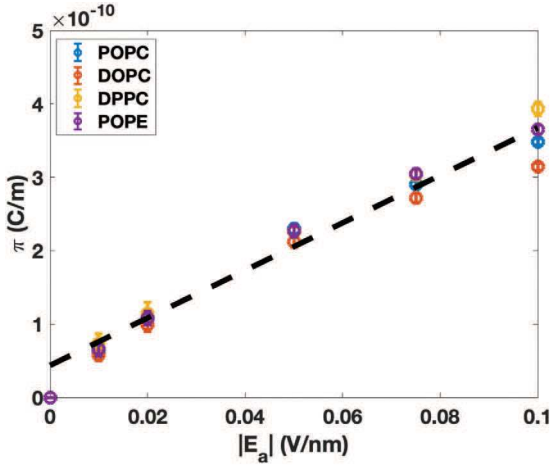

Fig. 10: The cumulative in-plane polarization density for the POPC, DOPC, DPPC and POPE bilayers obtained by adding the in-polarization densities of the lipid headgroup dipoles and the water dipoles in the headgroup/carbonyl regions. Addition of water polarisation leads to a nearly two-fold increase in the in-plane polarisation density.

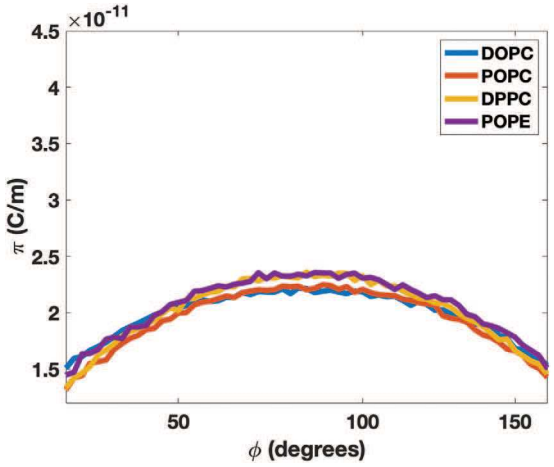

Fig. 11: The magnitude of the out-of-plane polarization density as we move along a meridian on the lipid vesicle subjected to 0.025 V/nm electric field. The out-of-plane polarization density is roughly half of the in-plane polarization density obtained in fig. 8(b).

applied electric field. This in turn implies that the bilayers possess a lower area per lipid and a lower permeability as the electric field is increased. Thus, the bilayers we simulated do not loose integrity in the presence of applied electric field. The slight jump observed for the DPPC bilayer at 0.1 V/nm in fig. S1 in the SM occurs due to the phase change induced by the lateral electric field [35].

Predictions from the coarse-grained simulations. To verify the estimates obtained from the all-atom systems, we performed coarse-grained simulations of a flat POPC bilayer in Martini (fig. 5). The inset in fig. 5 shows the coarse-grained headgroup dipole vector (orange vector) drawn from the PO4 bead to the NC3 bead. Figure 6 shows the in-plane polarization density obtained from the

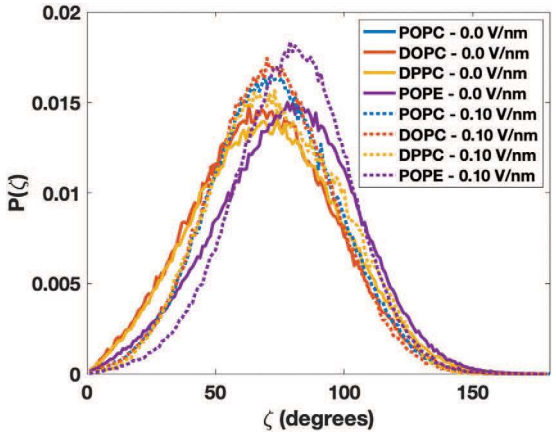

Fig. 12: Probability density distribution of the normal angle (ζ) made by the lipid dipoles (see fig. 2) in the absence and presence of electric field (0.10 V/nm). Application of electric field has minimal impact on the normal angle.

coarse-grained system. To facilitate comparison, we have reproduced the data from the all-atom systems in fig. 4. The data from the coarse-grained and the all-atom bilayers show very good agreement, confirming the ability of coarse-grained systems to adequately capture the electric-field–induced bilayer polarization.

Next, we simulated a 15nm radius vesicle to quantify the effect of bilayer curvature on the estimation of the in-plane flexoelectric coefficient. We constructed spherical vesicles for the four lipid types and subjected them to an electric field of 0.025 V/nm. Higher electric fields led to penetration of vesicles by water molecules, leading to electroporation as observed by Vernier and colleagues [5]. Figure 7 shows the deformed state of a POPC vesicle in the presence of the applied electric field. The inset shows a schematic of the lipid dipole vector, the applied electric field vector and their projected components on to the tangential plane of the bilayer surface.

Figure 8(a) shows the probability density $P(\theta)$ of the projected dipoles to align with the projected electric field $\mathbf{E}_t$. As before, in the absence of the electric field all angles have equal probability yielding the flat curves for the four lipid systems. In the presence of the electric field, the dipoles become oriented in the direction of $\mathbf{E}_t$ resulting in an increase in $P(\theta)$ at smaller angles and a decline at larger angles. The trend is consistent for the four lipid types. Next, we use eq. (1) to compute the in-plane polarization density from the projected dipole vectors in the bilayer. Figure 8(b) shows $|\boldsymbol{\pi}|$ as we move along a meridian from the north pole to the south pole of the simulated vesicle. We present the data for $20^\circ \leq \phi \leq 160^\circ$ due to high numerical error encountered in the close vicinity of the two poles because of the vanishing denominator in eq. (1). Figure 8(b) shows that around the two poles, the magnitude of in-plane polarization density is small. This is so because $\mathbf{E}_t$ is small and hence, the dipoles continue to have their rotational freedom. Around the equatorial

plane ($\phi \approx 90°$), the in-plane polarization density achieves its maximum value. In this region, $\mathbf{E}_t$ is maximum, which leads to the maximum alignment of lipid dipoles.

Finally, we use eq. (4) to calculate the in-plane flexoelectric coefficient for the four lipid systems. Figure 9 shows the predicted values as a function of the polar angle. The plots yield an average value of $5.5 \times 10^{17}\,\mathrm{Nm/C^2}$ for the in-plane flexoelectric coefficient for the different lipid types. These estimates are in very good agreement with the earlier estimate obtained from the atomistic simulations. Since both the flat bilayer and the vesicle geometries yield similar estimates, D is independent of membrane geometry, and hence, is purely a material property.

Conclusions. – In this study, we performed atomistic and coarse-grained molecular dynamics simulations to quantify the propensity of lipid bilayers to undergo in-plane polarization in the presence of an applied electric field. We used the numerical predictions to estimate the in-plane flexoelectric coefficient required to model the electromechanical response of lipid bilayers. Our results show that the in-plane flexoelectric coefficient $D \approx 5.5 \times 10^{17}\,\mathrm{Nm/C^2}$ for the four simulated lipid types. Despite the variations in the acyl chain saturation level and the headgroups structure, the four lipids show a comparable in-plane polarization.

Our study provides the first molecular proof of the in-plane polarization undergone by lipid bilayers in the presence of an applied electric field. The study shows that the bilayers undergo significant in-plane polarization, suggesting that in-plane polarization should be accounted for in analyzing the electromechanical response of bilayers in the presence of electric fields with tangential component. Furthermore, our study shows that the D estimate is independent of the bilayer geometry, confirming the assumption of a constant material property invoked in the new electromechanical theory [25]. Estimation of D overcomes a major roadblock that would allow future studies to numerically quantify the electromechanical response of membranes and validate modeling predictions with experimental data.

While in this study we invoked the in-plane polarization arising from the lipid dipoles in the headgroup region, reorientation of water molecule dipoles in the presence of electric field can change the net in-plane polarization developed in a bilayer. To quantify this effect, we computed the cumulative in-plane polarization density arising from the lipid dipoles and the water dipoles in the headgroup and the carbonyl regions. Figure 10 shows the $\pi - |E_a|$ data for the flat bilayer systems from the all-atom simulations. The addition of water dipoles is indeed able to generate an almost two-fold increase in the in-plane polarization density. This in turn would lead to a two-fold reduction in the effective in-plane flexoelectric coefficient.

Finally, several important remarks are in order here with reference to the previous models that invoke out-of-plane polarization. The out-of-plane polarization in these models mainly arises from a difference in the number of lipids in the two leaflets inside the control volume as the dipoles in the two leaflets are oriented in the opposite directions (see fig. 3 in [20]). Thus, for a flat bilayer, the net dipole in one leaflet cancels the net dipole in the other leaflet, leading to zero net polarization. In a curved bilayer, however, a net difference in the number of lipids in the two leaflets gives rise to a net out-of-plane polarization. To estimate this effect, we calculated out-of-plane polarization density and the flexoelectric coefficient for the Petrov model for our vesicle system subjected to $0.025\,\mathrm{V/nm}$ electric field. Our model yields a flexoelectric coefficient of $13.9 \times 10^{-20}\,\mathrm{C}$, which falls in the range of $3.1\text{–}1500 \times 10^{-20}\,\mathrm{C}$ documented in the literature [20,36–38]. Figure 11 shows the out-of-plane polarization developed along a meridian in the coarse-grained vesicles. Remarkably, the out-of-plane polarization is only half of the in-plane polarization in the presence of the same electric field (fig. 8(b)). This implies that for larger vesicles or membrane structure with smaller curvatures, the out-of-plane polarization would be much smaller compared to the in-plane polarization as the number of lipids in the two leaflets within the control will become comparable.

It is important to note that in contrast, the in-plane polarization is not intrinsically dependent on the bilayer curvature and the difference in the number of lipids in the two leaflets. The in-plane polarization is determined by the strength of the tangential electric field acting at any point on the bilayer surface and the realignment of the lipid dipoles. Thus, even a nearly flat bilayer can get polarized in the presence of an electric field. This is a fundamental difference between our model and the previous models. However, in the absence of an applied electric field, dipoles maintain rotational freedom and hence, curving of the bilayer does not lead to an in-plane polarization and the converse flexoelectric effect observed in the earlier models. Furthermore, our simulations show that the angle that the lipid dipoles make with the bilayer normal (ζ) undergoes minimal reorientation in the presence of the applied electric field (fig. 12), in stark contrast to the reorientation undergone by the tangential angle θ. This suggests that the electric field has a more dominant effect on the in-plane polarization as compared to out-of-plane polarization. It is therefore plausible that what was construed as the effect of out-of-plane polarization in the earlier studies could very well be the effect on in-plane polarization. Thus, there appears to be an impending need to revisit the basic tenets of electromechanical coupling in lipid bilayers through synergistic experimental and modeling studies.

* * *

AA acknowledges support from NSF Grants CMMI-1727271 and CMMI-1931084. The authors acknowledge the use of the Opuntia, Sabine, and Carya clusters to perform the simulations and the advanced technical support

from the Research Computing Data Core at UH to carry out the research presented here.

REFERENCES

[1] Nuccitelli R., *Curr. Top. Dev. Biol.*, **58** (2003) 1.

[2] Tai G., Tai M. and Zhao M., *Burns & Trauma*, **6** (2018), https://doi.org/10.1186/s41038-018-0123-2.

[3] Wang E., Zhao M., Forrester J. V. and McCaig C. D., *Investig. Ophthalmol. Vis. Sci.*, **44** (2003) 244.

[4] Sengel J. T. and Wallace M. I., *Proc. Natl. Acad. Sci. U.S.A.*, **113** (2016) 5281.

[5] Tokman M., Lee J. H., Levine Z. A., Ho M.-C., Colvin M. E. and Vernier P. T., *PLoS ONE*, **8** (2013) e61111.

[6] Polak A., Tarek M., Tomšič M., Valant J., Ulrih N. P., Jamnik A., Kramar P. and Miklavčič D., *Bioelectrochemistry*, **100** (2014) 18.

[7] Böckmann R. A., De Groot B. L., Kakorin S., Neumann E. and Grubmüller H., *Biophys. J.*, **95** (2008) 1837.

[8] Delemotte L. and Tarek M., *J. Membr. Biol.*, **245** (2012) 531.

[9] Hofmann G. A., Dev S., Dimmer S. and Nanda G., *IEEE Trans. Biomed. Eng.*, **46** (1999) 752.

[10] Jourabchi N., Beroukhim K., Tafti B. A., Kee S. T. and Lee E. W., *Gastrointest. Interv.*, **3** (2014) 8.

[11] Gothelf A., Mir L. M. and Gehl J., *Cancer Treat. Rev.*, **29** (2003) 371.

[12] Brownell W. E., Bader C. R., Bertrand D. and De Ribaupierre Y., *Science*, **227** (1985) 194.

[13] Raphael R. M., Popel A. S. and Brownell W. E., *Biophys. J.*, **78** (2000) 2844.

[14] Harland B., Lee W.-H., Brownell W. E., Sun S. X. and Spector A. A., *Med. Biol. Eng. Comput.*, **53** (2015) 405.

[15] Dimova R., Bezlyepkina N., Jordö M. D., Knorr R. L., Riske K. A., Staykova M., Vlahovska P. M., Yamamoto T., Yang P. and Lipowsky R., *Soft Matter*, **5** (2009) 3201.

[16] Dimova R., *Adv. Colloid Interface Sci.*, **208** (2014) 225.

[17] Vlahovska P. M., *Nonequilibrium dynamics of lipid membranes: Deformation and stability in electric fields*, in *Advances in Planar Lipid Bilayers and Liposomes*, Vol. **12** (Elsevier) 2010, pp. 101–146.

[18] Zhang J., Zahn J. D., Tan W. and Lin H., *Phys. Fluids*, **25** (2013) 071903.

[19] Todorov A., Petrov A. and Fendler J., *J. Phys. Chem.*, **98** (1994) 3076.

[20] Petrov A. G., *Biochim. Biophys. Acta - Biomembr.*, **1561** (2002) 1.

[21] Kummrow M. and Helfrich W., *Phys. Rev. A*, **44** (1991) 8356.

[22] Tu Z., Liu J., Xie Y. and Ou-yang Z.-C., *Geometric Methods in Elastic Theory of Membranes in Liquid Crystal Phases*, Vol. **2** (World Scientific) 2017.

[23] Mohammadi P., Liu L. and Sharma P., *J. Appl. Mech.*, **81** (2014) 011007.

[24] Gao L.-T., Feng X.-Q., Yin Y.-J. and Gao H., *J. Mech. Phys. Solids*, **56** (2008) 2844.

[25] Steigmann D. and Agrawal A., *Math. Mech. Complex Syst.*, **4** (2016) 31.

[26] Abtahi N., Bouzar L., Saidi-Amroun N. and Müller M. M., *EPL*, **131** (2020) 18001.

[27] Huang J., Rauscher S., Nawrocki G., Ran T., Feig M., de Groot B. L., Grubmüller H. and MacKerell A. D., *Nat. Methods*, **14** (2017) 71.

[28] Marrink S. J., Risselada H. J., Yefimov S., Tieleman D. P. and De Vries A. H., *J. Phys. Chem. B*, **111** (2007) 7812.

[29] Lee J., Cheng X., Swails J. M., Yeom M. S., Eastman P. K., Lemkul J. A., Wei S., Buckner J., Jeong J. C., Qi Y. *et al.*, *J. Chem. Theory Comput.*, **12** (2016) 405.

[30] Qi Y., Ingólfsson H. I., Cheng X., Lee J., Marrink S. J. and Im W., *J. Chem. Theory Comput.*, **11** (2015) 4486.

[31] Canham P. B., *J. Theor. Biol.*, **26** (1970) 61.

[32] Helfrich W., *Z. Naturforsch. C*, **28** (1973) 693.

[33] Jenkins J. T., *SIAM J. Appl. Math.*, **32** (1977) 755.

[34] Steigmann D. J., *Int. J. Non-Linear Mech.*, **56** (2013) 61.

[35] Thomas N. and Agrawal A., *Lateral electric field inhibits gel-to-fluid transition in lipid bilayers* (2021), https://www.biorxiv.org/content/10.1101/2021.01.29.428787v1.

[36] Petrov A. and Sokolov V., *Eur. Biophys. J.*, **13** (1986) 139.

[37] Todorov A., Petrov A., Brandt M. O. and Fendler J. H., *Langmuir*, **7** (1991) 3127.

[38] Petrov A. G., Miller B. A., Hristova K. and Usherwood P. N., *Eur. Biophys. J.*, **22** (1993) 289.